Literature Review

Matthew Gebert

March 13, 2020

Interfacing topological insulators surface states with ferroics

Contents

1 Introduction

In the last two decades there has been a vast discovery of new materials that exhibit phenomenal properties interesting for condensed matter physics research. Usually these materials are stumbled upon experimentally, however in the case of topological materials the setting and expectation was purely theoretical.

Topological insulators (TIs) attract interest because of their unique properties ~~related to electronics.~~ 2D and 3D ~~compounds~~ have edge and surface electronic states respectively, and these states exhibit useful properties such as momentum-spin locking (or localised spin densities) and suppressed back-scattering.

These properties may be used for applications like directing currents t~~hat are spinful, ie, exerting magnetic fields or used in spintronics~~, as well as providing currents that are robust with low resistance due to ensured conductivity.

This literature review aims to walk through the basics of TI materials

TO COMPLETE AFTER WRITING REVIEW

2 Topological insulator ~~history~~

2.1 History through Hall effects

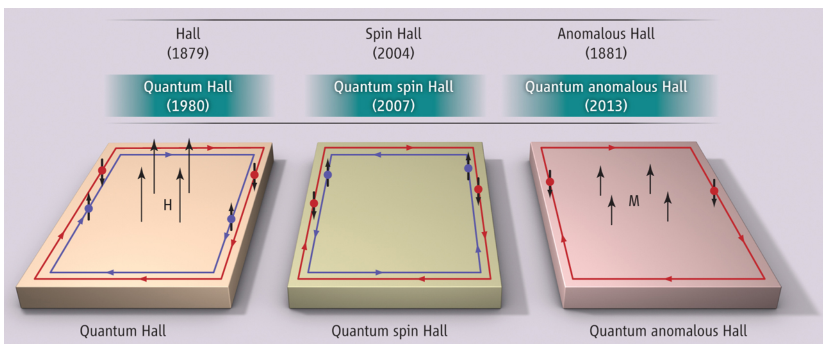

Figure 1: The three QH states discovered thus far [1]

2.1.1 Quantum Hall effect

The quantum hall effect (QHE) was first discovered in MOSFET [1] transistors 1980 [2], through a 2 dimensional electron gas (2DEG) found at the interface of a bulk semiconductor and the gate oxide.

Style needs to be changed

When introducing a magnetic field to materials, you can produce something called Landau quantisation. You can think of the physical mechanism as the quantisation of cyclotron orbits for charged particles in magnetic fields [2]. This has the effect of creating new bands called "Landau Levels", that each posses large numbers of orbitals. The degeneracy of the level goes as

$$\text{Degeneracy} = \frac{B \times A}{\phi_0} = \frac{B \times A}{h/e} \tag{1}$$

This means for some Fermi energy, that you can choose the magnetic field to appropriate values to fill these Landau levels.

[1] Metal-oxide semiconductor field effect transistors

[2] The reason for cyclotron orbits is due to the single valued electron wavefunction, ie $\oint \vec{P} \cdot d\vec{r} = 2\pi N$

better to introduce a diagram for Landau levels

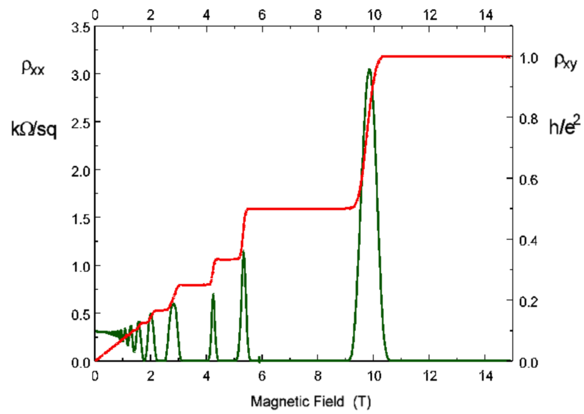

Figure 2: The quantum Hall effect.
Courtesy of D.R. Leadley, Warwick University 1997.

Not clear

~~The QHE looks finely tuned, but because of electrons interacting at the edge there is a confinement of edge states~~[3]. The edge states dominate transport when the Landau levels of the bulk are filled. Because they are dissipationless, the resistivity ρ_{xx} of the system vanishes, before reaching the next Landau level, where scattering between bulk states can occur again. This is the hallmark[3] of topological states, where there exists some states between different phases of matter.

The Hall resistivity ρ_{xy} exhibits quantised levels however.

$$\sigma_{xy} = \nu \frac{e^2}{h} \tag{2}$$

Thouless (~~who later received the~~ noble prize ~~in~~, 2016, ~~before passing away in 2019~~), Kohmoto, Nightingale, and den Nijs (TKNN)[4] where interested in gapped bulk systems but with conductive edges and a periodic lattice potential. These systems had been argued for explaining the QHE by Laughlin[5] and the integer effects had earlier been demonstrated theoretically by Hofstadter's Butterfly[6]. TKNN recognised that **K** space maps to a non-trivial Hilbert space for the QHE; the space has a topology. This topology can be specified by the integer ν which also corresponds to the hall conductance above in Eq. 2. In particular, their calculations only depended on details of the wavefunctions of the bandstructure.

Show calculation of berry phase of the Bloch wave function calculated around the BZ boundary divided by 2 pi

What makes this fascinating is that the QHE is a clear example of macroscopic quantum phenomena. Other such phenomena include Bose Einstein Condensation, where many atoms condense into the same uniform quantum state, and superconductivity where the pairing of electrons (Cooper pairs) also produce a new phase of macroscopic quantum behaviour.

For the QHE to occur, the Landau quantisation opens gaps in the band structure of the material, and the chemical potential is situated within this gap. In a classical picture, the boundaries of the material cannot sustain these cyclotron orbit, because of the phase transition to an ordinary insulator, rather than the QHE insulator, and so edge channels open in a **bulk-boundary correspondence**.

Note that the QHE does not preserve **time reversal** (TR) **symmetry**, as charge carriers experience different forces due to the magnetic field when their direction is inverted. The magnetic field breaks TR symmetry. You can see this in the two degrees of freedom in the system. For an out of plane magnetic field, charge is separated into two lanes, and those channels move a particular direction, ie forward above for electrons, backward below for holes. Reversing the direction of carriers yields the same channels but switched, forward above for holes, backward below for electrons.

[3] Although unrelated to the Hall effect, get the pun? Haha.

2.1.2 Quantum spin Hall effect

The spin hall was observed in 2004 by Kato *et al.*[7], where for particular semiconductors a spin density was observed rather than a charge density, like in the regular hall effect. The origins for such an phenomenon are similar to that of the quantum anomalous Hall effect in ferromagnets, sometimes being extrinsic, sometimes intrinsic. Intrinsically, the **Berry curvature** of the electronic valence-band Bloch wave functions result in spin-Hall effect.

The spin Hall insulator was proposed by Zhang's ~~group~~ et al.[8], where the **Berry phase** is finite implying a finite spin Hall conductivity. While this idea did not "generate spin currents due to an absence of any electrons at the Fermi level"[9], it allowed further exploration to find it quantised version, a quantum spin Hall (QSH) insulator[10;11;12].

In a real 1D system with spin, you have a regular four degrees of freedom; Spin can move either direction, and can move forward and backward. This could be separated into two copies of the QH system - spin up moving forward with spin down moving backward at the top, and spin down moving forward with spin up moving backward on the bottom. This is referred to the quantum spin Hall effect (QSHE). But what is the key ingredient that allows this separation of states to occur? In the QHE, it's the magnetic field that breaks time reversal symmetry. For QSH insulators, the essential ingredient is spin orbit coupling (SOC).

An important step made by Kane and Mele[11] was finding a "topological invariant" to characterise the QSH insulator states using an index. This index is called the Z_2 index. Topological invariants have appeared before. In the QHE, the TKNN invariant μ, where the quantised conductance is proportional to ν. The consequence of the Z_2 index is it maps the parity of the number of times the 1D edge state crosses the Fermi level. An odd parity ensures the existence of an edge state and consequently the phase of a topological insulator. The result is significant in it shows how topological phases exist in band structures of insulators, and do not require external magnetic fields breaking TRS like in the QHE[9].

Whilst Kane and Mele used their SOC model to investigate the bandgap opening of graphene, SOC is very difficult to experimentally detect in graphene due to the low coupling strength, compared to that of heavier species. Berneveig et al.[10] (Zhang's group) instead proposed a Z_2 model for the band structure of mercury telluride (HgTe). They predicted a CdTe/HgTe/CdTe quantum well would give rise to the QSH effect, when the HgTe layer reached a certain critical thickness. Experimental observation was confirmed soon thereafter by König[13], who observed a quantised conductivity σ_{xx} of $2e^2/h$, due to two conducting edges. They also observed the thickness dependence.

2.1.3 Topological insulators

By this time theorists (Moore & Balents[14], Fu, Kane and Mele[15]) had already leapt forward and predicted 3D systems that would exhibit quantum spin hall effects. It was at this point that the term "topological insulator" was first coined[14]. This is distinct to the 2D QSH insulators, but analogous in a 3D version. For these systems there was no longer one invariant to determine the topology of a system, but rather 4 separate invariants, for 16 classes of materials. Generally they could be separated into two groups - strong and weak 3D TIs.

The first prediction for a 3D TI was by Fu and Kane[16]. They predicted that the surface states of bismuth antimony ($Bi_{1-x}Sb_x$) could be observed by looking at angle resolved photo emission (ARPES, see 7.2.1). The signature for non-trivial topology was in observing surface states crossing the Fermi energy between two TR-invariant momenta[16] This was observed in the same system by Hsieh *et al.*[17].

2.1.4 Quantum anomalous Hall effect

Include some information on the discovery of the QAHE and the AHE, and it's relevance to both magnetic materials in addition to topological phases of matter.

2.2 Relevant theory and phenomena

2.2.1 Topological field theory

In 2001 the QHE state was generalised to a 4D TR-invariant state by Zhang and Hu, and was generalised by to field theory by Bernevig *et al.*. It was also shown later by Zhang how the Z_2 topology could be described in this field theory, and be reduced to the 2D and 3D cases.

Practically this is useful for describing electromagnetic response of TIs and predicting magneto-electric effects, according to Ando's review [9].

2.2.2 Dirac fermions

Within graphene, mentioned earlier for the Kane and Mele SOC model [12], the 2D electron gas over the carbon honeycomb lattice creates interesting band structure features called "Dirac cones". The carries occupying these band structure states behave according to a pseudo-relativistic Dirac equation, behaving differently to that of regular fermions in materials. Their physical behaviour mimics that of highly relativistic situations.

Dirac fermion mass :
Sometimes the charge carriers in graphene are called "massless" Dirac fermions - they behave analogous to relativistic particles with zero rest mass conforming to the Dirac equation [18]. This result comes from the observation of the fermions having a linear cyclotron mass with energy around the Dirac point's linear dispersion, effectively proving zero dependence on a "rest mass". Instead of their characteristic speed being the speed of light c, the Fermi velocity v_F describes their motion.

Generally in semiconductors and other insulators, the electronic bands eitherside of the bandgap become quite flat with curvature in momentum space. The important of such features is reflected in the effective mass of carriers as the Fermi energy locally fills states at the band edge. Historically, the effective mass of such carriers is calculated as [19]

$$m^* = \left(\frac{\partial E^2}{\partial^2 k}\right)^{-1} \tag{3}$$

For parabolic, isotropic bands, a local approximation to the effective mass is:

$$E(\mathbf{k}) = E_0 + \frac{\hbar^2 \mathbf{k}^2}{2m^*} \tag{4}$$

$$\tag{5}$$

which satisfies the above calculation. In graphene however, the dispersion equation near the Dirac cones (the K and K' points) are similar to the Dirac equation:

$$E(\mathbf{k}) \approxeq \hbar v_F \cdot \mathbf{k} \tag{6}$$

If we apply the same effective mass equation, we arrive at:

$$m^* = \left(\frac{\partial v_F \cdot \mathbf{k}}{\partial \mathbf{k}^2}\right)^{-1} \to \infty \tag{7}$$

If the carriers were really so heavy, conduction would be very restricted in Graphene. Instead, a different method of calculating the effective mass has to be used [20] avoiding divergence.

$$m^*(E, \mathbf{k}) = \frac{p}{v_g} = h^2 \mathbf{k} \left(\frac{\partial E}{\partial \mathbf{k}}\right)^{-1} \tag{8}$$

$$= hk\frac{1}{v_F} \tag{9}$$

This yields the mass proportional to the linear dispersion, exhibiting relativistic behaviour.

Dirac particles in topological insulators :
As pointed out by Ando[9], Spin-orbit interactions and 3D "massive" Dirac theory have been known for a long time in Bismuth research, which has also been a playground for it's diamagnetism (different to Pauli paramagnetism & diamagnetism). Wolff[21] showed that a 2 band bismuth model can be transformed into a 4-part Dirac Hamiltonian.

It's interesting that both Bismuth and another semi-metal antimony were used to produce the first 2D TI surface states in $Bi_{1-x}Sb_x$ where 2D surface "massless" Dirac systems exist. A distinguishing property of massless Dirac fermions is the Berry phase of π, which provides an absence of backscattering[22]. The TI surface states consequently electronically protected from some scattering.

3 Topological insulator theory

3.1 Berry Phase

Berry Connection is the ~~bra-ket~~ expectation value of a Gradient operator of vector $\vec{R}$ acting on a wavefunction over some path Γ with positions $\vec{R}$. Physically it is the mechanism from getting one geometric space point to another, ie the change of parameters.

$$\vec{\mathcal{A}}_n(\vec{R}) = i \langle \psi_n(\vec{R}) | \nabla_{\vec{R}} | \psi_n(\vec{R}) \rangle \tag{10}$$

This object has N parts, for each of the vector components. There's a different connection for every eigenstate, of every point in the space. It's a little more subtle than a vector - it transforms under Gauge transformations. For an example wavefunction to include some additional phase factor (i.e. Gauge transformation), the wavefunction transforms as $|\psi_n'(\vec{R})\rangle = e^{-i\beta(\vec{R})} |\psi_n(\vec{R})\rangle$. This results in a change for the Berry connection:

$$\vec{\mathcal{A}}_n'(\vec{R}) = \vec{\mathcal{A}}_n(\vec{R}) + \nabla_{\vec{R}}\beta(\vec{R}) \tag{11}$$

So the "connection" is that it transforms with the gradient of a function, like a vector potential.

Berry Curvature is the consequence or result of going from one set of starting parameters to the same set of parameters over some path (also called a **connection**). You could use the Schroedinger equation to provide a connection. It turns out that through evolution the state can pick-up a phase factor, relative to the original starting state. This phase factor is also known as the Berry phase[23], and has consequences for the quantum mechanical properties of the system.

The **Berry Phase** is the integral

$$\gamma_n(\Gamma) = \int_\Gamma \vec{\mathcal{A}}_n(\vec{R}) \cdot d\vec{R} \tag{12}$$

By changing the gauge of the Berry phase we can notice some properties that shift:

$$\gamma_n'(\Gamma) = \int_\Gamma \vec{\mathcal{A}}_n(\vec{R}) \cdot d\vec{R} + \int_\Gamma \nabla_{\vec{R}}\vec{\beta} \cdot d\vec{R} \tag{13}$$

$$\implies \gamma_n'(\Gamma) = \gamma_n(\Gamma) + \beta(R_f) - \beta(R_i) \tag{14}$$

It's not Gauge invariant, which makes it difficult to be useful for different measurements. However, if you begin **AND** end in the same configuration point (ie, a closed loop) then this value is Gauge invariant! This imposes a few restrictions on the system to achieve a result.

- Eigenstates have to be imaginary to achieve a non-zero Berry phase.
- If the path is 1D, then the integration cancels out to result in a zero Berry phase, again.

In 3D systems, the Berry phase over some path Γ enclosing a surface S, then Stokes theorem lets you specify the **Berry curvature**

$$\oint_{\Gamma} \vec{\mathcal{A}}_n \cdot d\vec{R} = \oiint_{S} \left(\nabla \times \vec{\mathcal{A}}\right) \cdot d\vec{S} \tag{15}$$

$$\vec{D} = \nabla_{\vec{R}} \times \vec{\mathcal{A}}_n(\vec{R}) \tag{16}$$

3.1.1 Aharonov–Bohm Effect

Todo: Fill out some basic theory and why the Berry phase solves this problem

3.2 Symmetries

3.2.1 Time-reversal symmetry

TODO: explain the role of TR symmetry

3.2.2 Inversion symmetry

Bulk states are spin-degenerate, because of combination of space-inversion symmetry ($E(k,\uparrow) = E(-k,\uparrow)$) and time-reversal symmetry ($E(k,\uparrow) = E(-k,\downarrow)$)[24]. At the surface however where inversion symmetry is broken, spin-orbit interaction can arise due to asymmetric electric fields and lift the spin degeneracy.

3.2.3 Particle-hole symmetry

TODO: explain the role of particle-hole symmetry

3.2.4 Sublattice symmetry

TODO: explain the role of sublattice symmetry

3.2.5 Kramers theorem

Kramers theorem requires particular points mapped from the BZ (Brouillin zone) to retain spin degeneracy. For $Bi_{1-x}Sb_x$, spin states split at the surface by spin-orbit interaction must remain spin-degenerate at four special TR invariant momenta; Γ, and three equivalent M points. Ref in Hsieh *et al.*[24].

3.3 Topological invariants

3.3.1 TKNN invariant

A detailed calculation for the TKNN invariant will be added in the future.

Simon first showed[25] that the Berry phase is significantly related to the TKNN topological invariant.

3.3.2 Z_2 invariant

A detailed calculation for this invariant will be added in the future.

3.3.3 Z_2 invariant in 3D

A detailed calculation for this invariant will be added in the future.

3.4 Spin-orbit coupling

Spin-orbit coupling (SOC) is coupling of both spin and orbital angular momentum properties of particles. Spin provides a magnetic moment, and the motion of the charged electron through its orbital angular momentum also provides a magnetic moment. From the electrons point of view, it can be considered to be the interaction of the electron's spin with the orbital motion of the nucleus, or through a crystal with a periodic potential.

Llewellyn Thomas derived the spin-orbit energy splitting for the hydrogen atom in 1926 [26;27]. You can derive the SOC from the Dirac equation for a spin $\frac{1}{2}$ particle in the presence of an electromagnetic field (ie, proton for hydrogen atom).

$$\left(E - mc^2\right)\psi = \left(\frac{p^2}{2m} - \frac{p^4}{8m^3c} + V - \frac{\hbar}{4m^2c^2}\frac{\partial V}{\partial r}\frac{\partial}{\partial r} + \frac{1}{2m^2c}\frac{1}{r}\frac{\partial V}{\partial r}\mathbf{S}\cdot\mathbf{L}\right)\psi \tag{17}$$

The first and third terms are the same as the non-relativistic Schrodinger equation, the second term is the relativistic correction, and the last term is the spin-orbit coupling.

You may also see the SOC represented by Hamiltonian terms such as

$$H_{SO} \propto \boldsymbol{\sigma} \cdot \left(\vec{\mathbf{E}} \times \vec{\mathbf{p}}\right) \tag{18}$$

where $\boldsymbol{\sigma}$ are the Pauli matrices, $\vec{\mathbf{E}}, \vec{\mathbf{p}}$ are the external electric field and momentum operator respectively. You can think of the momentum of the electron moving through the electric field as inducing a magnetic field interaction with the spin.

This coupling causes splitting, similar to Zeeman splitting, of electronic energy levels. For different atoms, the SOC is different, with the trend that heavier atoms have a larger SOC [28].

Add diagram of SOC strength of different atomic species

Within materials, SOC doesn't break time-reversal symmetry like magnetic field does for the QHE, but it can lead to the QSHE, where electrons differentiated by their spin move in opposite directions. Physical effects of SOC in most solid state materials typically result in the Rashba effect or the Dresselhaus effect [29]

3.4.1 Dresselhaus effect

The SOC for Bloch electrons (crystalline solid state) was first noted by Elliot and Dresselhaus [30]. Dresselhaus in particular demonstrated the SOC splitting of atomic orbitals could alter cyclotron resonance spectra in semiconductors, and went onto study type III-V and II-VI semiconductor structures in the early 1950's. The Dresselhaus effect occurs in crystals with bulk inversion asymmetry.

Inversion symmetry is when the crystal is symmetric under inversion, from some lattice point from the origin). The breaking of inversion symmetry (inversion asymmetry) is usually important in allowing non-linear effects to take place in materials, otherwise even harmonics of wave functions become suppressed. This includes materials that allow high harmonic generation, such as in ultra-fast femtosecond pulses [31].

Practically, the fact that net electric fields exist within crystals for particular crystal directions gives rise to spin-orbit interactions.

3.4.2 Rashba effect

Rashba studied a different type of crystal to Dresselhaus, known as a "wurtzite structure" in the late 1950's. His paper with Sheka demonstrated linear dispersion relationships near the Γ point. This paper (hard to come by online due to lack of translation and availability in the Soviet Union) is translated to English and included in Bihlmayer *et al.*[30]. The Rashba effect occurs in crystals also with net electric field; this one is due to structural inversion asymmetry, rather than bulk asymmetry. In particular systems such as those with uniaxial symmetry (in one axis only) such as the hexagonal crystals of cadmium-sulphur and cadmium-selenide where it was originally found by Rashba and Sheka.

Rashba-Edelstein Effect in Ferromagnetic Materials Todo: discuss some results of the Rashba effect in magnetic materials.

- `https://doi-org.ezproxy.lib.monash.edu.au/10.1016%2F0038-1098%2890%2990963-C`
- `https://doi-org.ezproxy.lib.monash.edu.au/10.1038%2Fnphys1362`
- `https://www-nature-com.ezproxy.lib.monash.edu.au/articles/nature13534`
- `https://advances.sciencemag.org/content/5/8/eaaw3415`
- `https://tms16.sciencesconf.org/data/pages/TI_lecture2.pdf`
- `https://arxiv.org/pdf/1401.0848.pdf`

3.5 Hamiltonians of TI Materials

The following models from Qi & Zhang[32] are formed for QSHE by a Hamiltonian that is a Taylor expansion in the wavevector **k** of interactions between highest and lowest conduction bands.

3.5.1 HeTe (Mercury Telluride)

$$H(\mathbf{k}) = \epsilon(k)\mathbb{1} + \begin{pmatrix} M(k) & A(k_x+ik_y) & 0 & 0 \\ A(k_x+ik_y) & -M(k) & 0 & 0 \\ 0 & 0 & M(k) & -A(k_x+ik_y) \\ 0 & 0 & -A(k_x+ik_y) & -M(k) \end{pmatrix} \tag{19}$$

with

$$\epsilon(k) = C + Dk^2, M(k) = M - Bk^2 \tag{20}$$

Here the upper 2x2 block describes the spin-up electrons in the s-like E1 conduction and p-like H1 valence bands. The lower 2x2 block describes the spin-down electrons in those same bands.

ϵ is the unimportant bending of all bands, where $\mathbb{1}$ is the identity matrix. The energy gap between the bands is $2M$, and B describes the curvature of the bands. A incorporates the inter-band coupling at lowest order. $M/B < 0$ has eigenstates of a trivial insulator. $M/B > 0, M$ becomes negative, and solution yields edge states of QSHE. You can also practise doing this with a 2D TI honeycomb lattice to gain explicit understanding like Kane and Mele[12;11].

Plot and display the eigenstates against momentum

3.5.2 Bi_2Te_3 (Bismuth Telluride)

$$H(\mathbf{k}) = \epsilon(k)\mathbb{1} + \begin{pmatrix} M(\mathbf{k}) & A(k_x+ik_y) & 0 & A_1k_z \\ A(k_x+ik_y) & -M(\mathbf{k}) & A_1k_z & 0 \\ 0 & A_1k_z & M(\mathbf{k}) & -A(k_x+ik_y) \\ A_1k_z & 0 & -A(k_x+ik_y) & -M(\mathbf{k}) \end{pmatrix} \tag{21}$$

with

$$\epsilon(k) = C + D_1k_z^2 + D_2k_\perp^2, M(k) = M - B_1k_z^2 - B_2k_\perp^2 \tag{22}$$

Bi_2Te_3 follows a similar model, in the context of bonding and anti-bonding p_z orbitals with both spins. B_1 and B_2 have the same sign, and as before, depending on the sign of M, the bands undergo inversion.

It is essential to be in 3D to be able to construct a single Dirac cone for a 2D surface - the degeneracy of graphene with six Dirac cones makes it clear. The 2D HgTe quantum well at the crossover point $d = d_c$ also has two Dirac cones.

4 Topological insulator materials

4.1 Materials & Growths

4.1.1 Bi_2Se_3

Kim *et al.*[33] - Observation of zero hall coefficient at the Dirac point - rather than divergence with lack of carriers.

$$R_H = \frac{E_y}{j_x B_z} \tag{23}$$

4.1.2 Bi_2Te_3

4.1.3

5 Magnetic materials

For further information to include, read the following topical review article: [34]

5.1 Macroscopic magnetic classifications

5.1.1 Ferromagnetic

Ferromagnetism is the strongest form of natural macroscopic magnetism, used in common everyday applications, such as refrigerator magnets or compass needles. There are commonly made up of compounds containing iron, cobalt, nickel or rare earth metals. There are two classes of ferromagnetic materials, “soft” and “hard”, depending on their ability to have their microcrystalline structure polarised after manufacturing.

In 1948 Louis Néel showed that at a microscopic level, not only can ferromagnetism result from the alignment of magnetic moments but also can result from magnetisation where some moments point in the opposite direction (ferrimagnetism)[35], however due to different contributions a net magnetisation remains.

5.1.2 Anti-ferromagnetic

As identified by Néel for ferrimagnetic materials, the magnetic ordering where neighbouring spins are misaligned can also cancel out any net magnetisation resulting in an anti-ferromagnetic material. However, above a particular temperature (dubbed the Néel temperature), the material undergoes a phase change and typically becomes paramagnetic due to the freedom for spins to be flipped. There can be multiple ground states for spin systems, compared to the uniform case of a strict ferromagnet. This is referred to as a ”geometric frustration”, in that a system doesn’t find a single ground state.

5.1.3 Paramagnetic

Paramagnetism is a material that induces a weak magnetic field in the direction of an applied field. It is due to the unpaired electrons in atoms with unfilled bands.

5.1.4 Diamagnetic

Diamagnetism on the other hand is the induction of an opposing magnetic field that repels the applied field. It is generally the result of static electrons that can screen changes in magnetic flux by acting like little current loops. It's effect is present in ferromagnetic and paramagnetic materials, but it's effect weak in comparison and so does not dominate the magnetisation dynamics. Langevin diamagnetism and Landau diamagnetism govern the dynamics of localised and metallic electrons respectively. To fill out at a later date

5.2 Microscopic magnetic phenomena

Magnetism has taken a while to be understood at its quantum, microscopic level, and still poses many questions today. Spin orbit coupling has already been discussed in Sec 3.4, but here we will cover other phenomena that contribute to atomic scale magnetic phenomena.

5.2.1 Quantum-mechanical exchange

To fill out at a later date

5.2.2 Crystal-field interaction

To fill out at a later date

5.3 Spintronics prior to topological insulators

To include at a later date, a history on spin effects in materials and the motivations towards spintronics pre-2000s, including some SOC further progress outside of TIs. Checkout Rashba's review from 1965[36], and some more modern ones.

5.4 Ferromagnetic Insualtors

NEED TO FILL OUT THIS SECTION ALOT Ferromagnetic insulators (FIs) are rare, because most magnetic materials that incorporate iron, cobalt or nickel are often conductive. That being said, some 3D FIs have been known for a while, and recently some new FIs that can be exfoliated down to thin flakes have been discovered.

5.4.1 3D FIs

$BaFe_{12}O_{19}$ (BFO) can be prepared by ALD, and can be grown to less than 5nm[37].

$Y_3Fe_5O_{12}$ (YIG) is also a bulk film that can be grown thinly, for example down to 30nm in Wang *et al.*[38].

5.4.2 2D FIs

Chromium triiodide (CrI_3) was first reported on around 2014[39]. Recently reports show it's ferromagnetic properties down to few-layers[40;41].

- `https://pubs-acs-org.ezproxy.lib.monash.edu.au/doi/abs/10.1021/cm504242t?src=recsys`
- `https://www-nature-com.ezproxy.lib.monash.edu.au/articles/nature22391`
- `https://www-nature-com.ezproxy.lib.monash.edu.au/articles/s41565-018-0121-3`

$Cr_2Ge_2Te_6$ (CGT) is also a new thin ferromagnetic insulator. It consists of quintuble players, similar to Bi_2Te_3 or Bi_2Se_3, and is also terminated with hexagonal Te planes. The discovery paper of 2017[42] shows that bilayers are stable for exfoliation. Whilst the bulk material has a Curie temperature (todo - define the curie temperature) of 61K, the 2D material is well defined below 40K.

$MgTiO_3$ (MTO) is another recent addition to thin film ferromagnetic insulator films[43].
Todo: discuss lattice matching in heterostructures page?

6 TI & FI heterostructures

6.1 Theory

6.2 Spin Torque

6.2.1 Torque

6.2.2 Spin Torque Angle - Spin Torque Efficiency

6.2.3 Magnetization

Larmor Equation:

$$\vec{T} = \mu_0 \vec{\mathbf{M}} \times \vec{\mathbf{H}} \tag{24}$$

Torque:

$$\frac{d\vec{L}}{dt} = \vec{T} \tag{25}$$

Gyromagnetic Ratio

$$\gamma \equiv \frac{\mu}{L} \tag{26}$$

Magnetization Change

$$\frac{d\vec{M}}{dt} = \gamma \vec{T} \tag{27}$$

6.2.4 Critical Current Density

6.2.5 Charge Spin Conversion Efficiency

6.3 Experiments

TODO: go through past experiments. Take significant of results, sample fabrication, experimental methodology.

6.3.1 Conductive films (non-insulating)

- (2012) Liu et al. Beta-Ta with CoFeB (Observed Torque, 2.1mT for 0.7mA, Sputtered/evaporated onto surfaces)
- (Apr 2013) Chang et al. Observation of QAHE - Cr0.15(Bi0.1Sb0.9)1.85Te3 - 5 quintuple layers, on SrTiO3, grown through MBE. Mobilities lower than 1000cm2/Vs. Chromium doping to make ferromagnetic, RHEED, ARPES.

- (Apr 2014) Y. Fan et al. Epitaxial (Bi0.5Sb0.5)2Te3/(Cr0.08Bi0.54Sb0.38)2Te3 bilayer films, 3 & 6 Quintuple layers respectively. AHE. (θSH reported to be very large??). Look again at device fab.
- (2014) A.R. Mellnik et al. 8nm Bi2Se3 and 8nm / 16nm Ni81Fe19 Bilayer (MBE & Sputtering) (Observed Torque Applied, Torque per unit moment Tparallel = 2.7 x 10-5, T¬perp=3.7 x 10-5), ωSH_parallel=(2.0 ± 0.4) × 105/2e ω-1 m-1 and σSH_perp = (1.6 ± 0.2) × 105/2e ω-1 m-1
- (2016) P. Li et al. Pt/BaFe12O19 – Torque observed, value not mentioned.
- (Aug 2017) J. Han et al. (MIT & Samarth Grp) - GaAs / Bi2Se3(7.4nm)/CoTb(4.6nm)/SiNx(3 nm) - Magnetron and MBE. Critical current density 2.8 x 106 A/cm^2. 0.16 effective SH angle. Large discrepancies noted in this paper. Also searched (Bi, Sb)2Te3, and compared to Pt and other heavy metals.
- (Sep 2017) K. Yasuda et al. Crx(Bi1-ySby)2-xTe3/(Bi1-ySby)2Te3 - Magnetic non-magnetic heterostructures. Second Harmonic Voltage goverened by asymmetric magnon scattering gives incorrect value of CSC (Charge spin conversion efficiency).
- **(Nov 2017) Y. Wang et al. Bi2Se3/NiFe Heterostructure, Describes contamination of BS, 2DEG to the SOT effects from TSS affecting Bi2Se3 systems. Also used Bi2Se3/Co40Fe40B20, and Bi2Se3 (8 QL)/Py(6nm). Growths on Al2O3. Used MgO and Al2O3 to protect. Also SiO2 used for Py devices. Iron Milling used with Photolithography.**
- (Jul 2018) Khang et al. Bi0.9Sb0.1, 5/10nm Mn0.45Ga0.55 3nm layers $\sigma \approx 2.5 \times 10^5 \omega^{-1} m^{-1}, \theta_{SH} \approx 52$ and $\theta_{SH} \approx 1.3 \times 10^7 \hbar/2e\omega^{-1}m^{-1}$
- (Jul 2018) Mahendra DC et al. BixSe(1-x)/Co20Fe60B20 (Magentron Sputtered) θ_S = 18.62 (d.c. planar Hall) &8.67 (ST-FMR) [Si/SiO2/MgO (2nm)/BixSe(1-x)(tBS nm)/ CoFeB(5nm)/MgO(2nm)/Ta(5nm)] tBS=4,6,8,16,40nm
- (Jan 2018) Y. Li et al. Epitaxial (001) SmB6/Si thin films (50nm +) with MgO(1.5)/CFB(Co40Fe40B20, 1)/$\beta - W(0.8)$ – DC Magnetron sputtering / DC&RF magnetron...

6.3.2 Insulating Films

- (2019) P. Li et al. Bi2Se3 and FI - BaFe12O19 https://advances.sciencemag.org/content/5/8/eaaw3415
- YIG (2016) H. Wang et al. https://journals-aps-org.ezproxy.lib.monash.edu.au/prl/pdf/10.1103/PhysRevLett.117.076601

6.4 Non-TI Devices

- (2010) Co layer 0.6nm, with Pt 3nm and AlO_x layers 2nm, transverse magnetic fields. https://www-nature-com.ezproxy.lib.monash.edu.au/articles/nmat2613?proof=trueMay

7 Experimental methods

7.1 Synthesis, Growth and Fabrication

TODO: fill in with summary of previous growth methods and experimental methods used for heterostructures.

7.1.1 MBE Growths

7.2 Spectroscopic Metrological Methods

7.2.1 ARPES

For material characterisation, angle resolved photo-emission spectroscopy (ARPES) is a method of resolving the ejection of electrons from a material by high energy photons. Analysis of the momentum of the incident and emission resolve the electronic band structure.

There now exist a variety of different ARPES methods that can be employed in understanding the electronic structure of materials; these include "soft-X-ray ARPES, time-resolved ARPES, spin-resolved ARPES and spatially resolved ARPES" [44]. The progress fo UV and soft-X-ray synchrotron light sources make it possible to distinguish between bulk and surface states for TI materials. Spin detectors determine the spin state of emitted electrons, allowing insight into spin-textures of surface states. Time-resolved ARPES (using femtosecond pulses) allows observation of "ultrafast electronic dynamics and states above the chemical potential" [44]. Finally, spatially resolved ARPES can be used to pinpoint sub-micron scale features, particularly if you want to distinguish between phases, or across material gradients (such as gradient MBE growths).

Spin Resolved ARPES The first spin resolved (SR) ARPES that yielded the direct observation of helical spin-polarization was done by Hsieh *et al.* [24] at the end of 2008, again in $Bi_{1-x}Sb_x$, followed with more detailed results by Nishide *et al.* [45].

In these experiments, topological details could be found by studying the surface band-dispersion and their respective spin polarizations. For example, the fact that there are 5 bands implies that an odd number of Fermi-surfaces enclose the spin-degenerate K points. This gives rise to determining the topological quantum number $\nu_0 = 1$ (0 if even).

7.2.2 Spin polarized STS

The first scanning tunelling spectropscopy (STS) study on $Bi_{1-x}Sb_x$ was published in 2009 by Roushan *et al.* [46] who detected the absense of backscattering even with strong system disorder. By taking fourier transforms of the surface state data they take, they can infer scattering information and lattice information. Combining this with spin-resolved ARPES they could determine the spin dependent scattering probability, and match their STS measurements to 95%. Doing the same with spin-independent scattering yields a match of only 80%.

7.3 Transport Metrological Methods

Test

7.3.1 Quantum Oscillations

Taskin & Ando [47] used quantum behaviour reported in Bi and $Bi_{1-x}Sb_x$ to differentiate between coherent electronic transport (edge states) and incoherent transport within an impurity band. The measurements (along with magnetic & resistivity measurements) where implemented using "de Haas-van Alphen (dHvA)" methodology. To do this, you measure the magnetization M across magnetic field strengths B. They also measured for different direction of the sample.

The derivative of the both ρ_{xx} and ρ_{xx} with respect to B, plotted against $1/B$ show Shubnikov-de Haas (SdH) oscillations below 2T field strenght. This is a quantum effect, and consequently is argued that it comes from a well-defined Fermi surface, not some impurity band which wouldn't be stable. The previous measurements of the resistivity with different doping proportions confirmed the insulating nature of the samples.

7.3.2 Magnetization

Taskin & Ando[47] measured DC magnetization using a SQUID magnetometer.

8 Related knowledge & concepts

8.1 Symmetry

Symmetry is very important in all physical systems. For example, the order exhibited in crystals can be described through the breaking of the continuous (rotational & translational) symmetry of space. This is due to the electrostatic interactions that cause a periodic lattice. In Magnets, spin space and time reversal symmetry are broken.

8.1.1 Symmetry points

In solid state physics, when observing the reciprocal space for the dispersion relations, there exist particular symmetry points, such as the Γ point, K points, M points and so forth. These have importance in the behaviour of materials due to their propagation vectors through the crystal.

Not sure if this is entirely correct.

General	
Γ	Center of the Brillouin zone
Simple cube	
M	Center of an edge
R	Corner point
X	Center of a face
Face-centered cubic	
K	Middle of an edge joining two hexagonal faces
L	Center of a hexagonal face
U	Middle of an edge joining a hexagonal and a square face
W	Corner point
X	Center of a square face
Body-centered cubic	
H	Corner point joining four edges
N	Center of a face
P	Corner point joining three edges
Hexagonal	
A	Center of a hexagonal face
H	Corner point
K	Middle of an edge joining two rectangular faces
L	Middle of an edge joining a hexagonal and a rectangular face
M	Center of a rectangular face

8.2 Fine Structure Constant

The fine structure constant, also known as Sommerfields constant, is the coupleing constant "α" that measures the strength of the EM force interacting with light.

Two methods it has been measured by include the anomalous magnetic moment of the electron, a_e, as well as appearing in the Quantum Hall Effect (QHE).

It was originally introduced by Summerfieldas a theoretical correction to the Bohr model, explaining fine structure through elliptical orbits and relitivistic mass-velocity.

8.3 Hamiltonians of Crystal Lattices

Turns out that you can describe the hamiltonian of the electrons in a crystal lattice. For this, there exists first quantisation, second quantisation hamiltonian.

- First quantisation - The classical particles are assigned wave amplitudes. This is "semi-classical" where only the particles or objects are treated using quantum wavefunctions, but environment is classical.
- Second quantisation (Canonical Quantisation, occupation number representation) - The wave fields are "quantized" to describe the problem in terms of "quanta" or particles. This usually means referring to a wavefunction of a state, described the the vacuum state with a series of creation operators to create the current state. Fields are now treated as field operators, similar to how physical quantities (momentum, position) are thought of as operators in first quantisation.

9 Quotes

Finally we introduce the parameter of which all the fuss is about.

R.F. Hofstadter, *[6]*

10 Questions to Answer

- SOC - Why only in heavier elements? Explain properly. Also, why think relativistically? Motion of electron means magnetic field observed?
- Spin is in the 2D surface plane of a 3D TI, always perpendicular to that of the momentum - how can I couple a ferromagnetic material if there's no out-of plane?
- ARPES - how can this be used to verify the surface states of TI materials? (and differentiate from the bulk).
- Dirac Cones - why do these only appear in 2D systems.
- Why is spin-polarization called "Helical" spin polarization?

11 Bibliography

[1] Seongshik Oh. The Complete Quantum Hall Trio. *Science*, 340(6129):153–154, April 2013. ISSN 0036-8075, 1095-9203. doi: 10.1126/science.1237215. URL `http://science.sciencemag.org.ezproxy.lib.monash.edu.au/content/340/6129/153`.

[2] K. v. Klitzing, G. Dorda, and M. Pepper. New Method for High-Accuracy Determination of the Fine-Structure Constant Based on Quantized Hall Resistance. *Physical Review Letters*, 45(6): 494–497, August 1980. doi: 10.1103/PhysRevLett.45.494. URL `https://link.aps.org/doi/10.1103/PhysRevLett.45.494`. Publisher: American Physical Society.

[3] F. Duncan M. Haldane. Topological Quantum Matter. *International Journal of Modern Physics B*, 32(13):1830004, May 2018. ISSN 0217-9792, 1793-6578. doi: 10.1142/S0217979218300049. URL `https://www.worldscientific.com/doi/abs/10.1142/S0217979218300049`.

[4] D. J. Thouless, M. Kohmoto, M. P. Nightingale, and M. den Nijs. Quantized Hall Conductance in a Two-Dimensional Periodic Potential. *Physical Review Letters*, 49(6):405–408, August 1982. doi: 10.1103/PhysRevLett.49.405. URL `https://link.aps.org/doi/10.1103/PhysRevLett.49.405`. Publisher: American Physical Society.

[5] R. B. Laughlin. Quantized Hall conductivity in two dimensions. *Physical Review B*, 23(10): 5632–5633, May 1981. doi: 10.1103/PhysRevB.23.5632. URL `https://link.aps.org/doi/10.1103/PhysRevB.23.5632`. Publisher: American Physical Society.

[6] Douglas R. Hofstadter. Energy levels and wave functions of Bloch electrons in rational and irrational magnetic fields. *Physical Review B*, 14(6):2239–2249, September 1976. ISSN 0556-2805. doi: 10.1103/PhysRevB.14.2239. URL `https://link.aps.org/doi/10.1103/PhysRevB.14.2239`.

[7] Y. K. Kato, R. C. Myers, A. C. Gossard, and D. D. Awschalom. Observation of the Spin Hall Effect in Semiconductors. *Science*, 306(5703):1910–1913, December 2004. ISSN 0036-8075, 1095-9203. doi: 10.1126/science.1105514. URL `http://science.sciencemag.org/content/306/5703/1910`.

[8] Shuichi Murakami, Naoto Nagaosa, and Shou-Cheng Zhang. Spin-Hall Insulator. *Physical Review Letters*, 93(15):156804, October 2004. ISSN 0031-9007, 1079-7114. doi: 10.1103/PhysRevLett.93.156804. URL `https://link.aps.org/doi/10.1103/PhysRevLett.93.156804`.

[9] Yoichi Ando. Topological Insulator Materials. *Journal of the Physical Society of Japan*, 82 (10):102001, October 2013. ISSN 0031-9015, 1347-4073. doi: 10.7566/JPSJ.82.102001. URL `http://arxiv.org/abs/1304.5693`. arXiv: 1304.5693.

[10] B. Andrei Bernevig, Taylor L. Hughes, and Shou-Cheng Zhang. Quantum Spin Hall Effect and Topological Phase Transition in HgTe Quantum Wells. *Science*, 314(5806):1757–1761, December 2006. ISSN 0036-8075, 1095-9203. doi: 10.1126/science.1133734. URL `http://science.sciencemag.org/content/314/5806/1757`. Publisher: American Association for the Advancement of Science Section: Report.

[11] C. L. Kane and E. J. Mele. Z 2 Topological Order and the Quantum Spin Hall Effect. *Physical Review Letters*, 95(14), September 2005. ISSN 0031-9007, 1079-7114. doi: 10.1103/PhysRevLett.95.146802. URL `https://link.aps.org/doi/10.1103/PhysRevLett.95.146802`.

[12] C. L. Kane and E. J. Mele. Quantum Spin Hall Effect in Graphene. *Physical Review Letters*, 95 (22):226801, November 2005. doi: 10.1103/PhysRevLett.95.226801. URL `https://link.aps.org/doi/10.1103/PhysRevLett.95.226801`.

[13] Markus König, Steffen Wiedmann, Christoph Brüne, Andreas Roth, Hartmut Buhmann, Laurens W. Molenkamp, Xiao-Liang Qi, and Shou-Cheng Zhang. Quantum Spin Hall Insulator State in HgTe Quantum Wells. *Science*, 318(5851):766–770, November 2007. ISSN 0036-8075, 1095-9203. doi: 10.1126/science.1148047. URL `http://science.sciencemag.org/content/318/5851/766`.

[14] J. E. Moore and L. Balents. Topological invariants of time-reversal-invariant band structures. *Physical Review B*, 75(12):121306, March 2007. doi: 10.1103/PhysRevB.75.121306. URL `https://link.aps.org/doi/10.1103/PhysRevB.75.121306`.

[15] Liang Fu, C. L. Kane, and E. J. Mele. Topological Insulators in Three Dimensions. *Physical Review Letters*, 98(10):106803, March 2007. doi: 10.1103/PhysRevLett.98.106803. URL `https://link.aps.org/doi/10.1103/PhysRevLett.98.106803`.

[16] Liang Fu and C. L. Kane. Topological insulators with inversion symmetry. *Physical Review B*, 76(4):045302, July 2007. doi: 10.1103/PhysRevB.76.045302. URL `https://link.aps.org/doi/10.1103/PhysRevB.76.045302`. Publisher: American Physical Society.

[17] D. Hsieh, D. Qian, L. Wray, Y. Xia, Y. S. Hor, R. J. Cava, and M. Z. Hasan. A topological Dirac insulator in a quantum spin Hall phase. *Nature*, 452(7190):970–974, April 2008. ISSN 1476-4687. doi: 10.1038/nature06843. URL `http://www.nature.com/articles/nature06843`.

[18] K. S. Novoselov, A. K. Geim, S. V. Morozov, D. Jiang, M. I. Katsnelson, I. V. Grigorieva, S. V. Dubonos, and A. A. Firsov. Two-dimensional gas of massless Dirac fermions in graphene. *Nature*, 438(7065):197–200, November 2005. ISSN 1476-4687. doi: 10.1038/nature04233. URL `http://www.nature.com/articles/nature04233`. Number: 7065 Publisher: Nature Publishing Group.

[19] Charles Kittel. Introduction to Solid State Physics, 8th Edition | Wiley. URL `https://www.wiley.com/en-au/Introduction+to+Solid+State+Physics%2C+8th+Edition-p-9780471415268`. Library Catalog: www.wiley.com.

[20] V. Ariel and A. Natan. Electron effective mass in graphene. In *2013 International Conference on Electromagnetics in Advanced Applications (ICEAA)*, pages 696–698, Torino (Turin), Italy, September 2013. IEEE. ISBN 978-1-4673-5707-4 978-1-4673-5705-0. doi: 10.1109/ICEAA.2013.6632334. URL `http://ieeexplore.ieee.org/document/6632334/`.

[21] P. A. Wolff. Matrix elements and selection rules for the two-band model of bismuth. *Journal of Physics and Chemistry of Solids*, 25(10):1057–1068, October 1964. ISSN 0022-3697. doi: 10.1016/0022-3697(64)90128-3. URL `http://www.sciencedirect.com/science/article/pii/0022369764901283`.

[22] Tsuneya Ando, Takeshi Nakanishi, and Riichiro Saito. Berry's Phase and Absence of Back Scattering in Carbon Nanotubes. *Journal of the Physical Society of Japan*, 67(8):2857–2862, August 1998. ISSN 0031-9015. doi: 10.1143/JPSJ.67.2857. URL `https://journals.jps.jp/doi/abs/10.1143/JPSJ.67.2857`. Publisher: The Physical Society of Japan.

[23] M V Berry. Quantal Phase Factors Accompanying Adiabatic Changes. *Proceedings of the Royal Society of London. Series A, Mathematical and Physical Sciences*, 392(1802):14, March 1984.

[24] D. Hsieh, Y. Xia, L. Wray, D. Qian, A. Pal, J. H. Dil, J. Osterwalder, F. Meier, G. Bihlmayer, C. L. Kane, Y. S. Hor, R. J. Cava, and M. Z. Hasan. Observation of Unconventional Quantum Spin Textures in Topological Insulators. *Science*, 323(5916):919–922, February 2009. ISSN 0036-8075, 1095-9203. doi: 10.1126/science.1167733. URL `http://science.sciencemag.org/content/323/5916/919`.

[25] Barry Simon. Holonomy, the Quantum Adiabatic Theorem, and Berry's Phase. *Physical Review Letters*, 51(24):2167–2170, December 1983. doi: 10.1103/PhysRevLett.51.2167. URL `https://link.aps.org/doi/10.1103/PhysRevLett.51.2167`. Publisher: American Physical Society.

[26] L. H. Thomas. The Motion of the Spinning Electron. *Nature*, 117(2945):514–514, April 1926. ISSN 1476-4687. doi: 10.1038/117514a0. URL `http://www.nature.com/articles/117514a0`. Number: 2945 Publisher: Nature Publishing Group.

[27] L.H. Thomas. The kinematics of an electron with an axis. *The London, Edinburgh, and Dublin Philosophical Magazine and Journal of Science*, 3(13):1–22, January 1927. ISSN 1941-5982, 1941-5990. doi: 10.1080/14786440108564170. URL `http://www.tandfonline.com/doi/abs/10.1080/14786440108564170`.

[28] Frank Herman, Charles D. Kuglin, Kermit F. Cuff, and Richard L. Kortum. Relativistic Corrections to the Band Structure of Tetrahedrally Bonded Semiconductors. *Physical Review Letters*, 11(12):541–545, December 1963. ISSN 0031-9007. doi: 10.1103/PhysRevLett.11.541. URL `https://link.aps.org/doi/10.1103/PhysRevLett.11.541`.

[29] S. Majumdar, H. S. Majumdar, and R. Österbacka. 1.05 - Organic Spintronics. In David L. Andrews, Gregory D. Scholes, and Gary P. Wiederrecht, editors, *Comprehensive Nanoscience and Technology*, pages 109–142. Academic Press, Amsterdam, January 2011. ISBN 978-0-12-374396-1. doi: 10.1016/B978-0-12-374396-1.00023-4. URL `http://www.sciencedirect.com/science/article/pii/B9780123743961000234`.

[30] G Bihlmayer, O Rader, and R Winkler. Focus on the Rashba effect. *New Journal of Physics*, 17(5):050202, May 2015. ISSN 1367-2630. doi: 10.1088/1367-2630/17/5/050202. URL `http://stacks.iop.org/1367-2630/17/i=5/a=050202?key=crossref.4b499e8c976ab70d1dc90ec00e1cc9ef`.

[31] Tenio Popmintchev, Ming-Chang Chen, Dimitar Popmintchev, Paul Arpin, Susannah Brown, Skirmantas Ališauskas, Giedrius Andriukaitis, Tadas Balčiunas, Oliver D. Mücke, Audrius Pugzlys, Andrius Baltuška, Bonggu Shim, Samuel E. Schrauth, Alexander Gaeta, Carlos Hernández-García, Luis Plaja, Andreas Becker, Agnieszka Jaron-Becker, Margaret M. Murnane, and Henry C. Kapteyn. Bright Coherent Ultrahigh Harmonics in the keV X-ray Regime from Mid-Infrared Femtosecond Lasers. *Science*, 336(6086):1287–1291, June 2012. ISSN 0036-8075, 1095-9203. doi: 10.1126/science.1218497. URL `http://science.sciencemag.org/content/336/6086/1287`. Publisher: American Association for the Advancement of Science Section: Report.

[32] Xiao-Liang Qi and Shou-Cheng Zhang. The quantum spin Hall effect and topological insulators. *Physics Today*, 63(1):33–38, January 2010. ISSN 0031-9228, 1945-0699. doi: 10.1063/1.3293411. URL `http://physicstoday.scitation.org/doi/10.1063/1.3293411`.

[33] Dohun Kim, Sungjae Cho, Nicholas P. Butch, Paul Syers, Kevin Kirshenbaum, Shaffique Adam, Johnpierre Paglione, and Michael S. Fuhrer. Surface conduction of topological Dirac electrons in bulk insulating Bi 2 Se 3. *Nature Physics*, 8(6):459–463, June 2012. ISSN 1745-2481. doi: 10.1038/nphys2286. URL `http://www.nature.com/articles/nphys2286`. Number: 6 Publisher: Nature Publishing Group.

[34] R. Skomski. Nanomagnetics. *Journal of Physics: Condensed Matter*, 15(20):R841–R896, May 2003. ISSN 0953-8984. doi: 10.1088/0953-8984/15/20/202. URL `https://doi.org/10.1088%2F0953-8984%2F15%2F20%2F202`. Publisher: IOP Publishing.

[35] M. Louis Néel. Propriétés magnétiques des ferrites ; ferrimagnétisme et antiferromagnétisme. *Annales de Physique*, 12(3):137–198, 1948. ISSN 0003-4169, 1286-4838. doi: 10.1051/anphys/194812030137. URL `https://www.annphys.org/articles/anphys/abs/1948/03/anphys19481203p137/anphys19481203p137.html`. Number: 3 Publisher: EDP Sciences.

[36] É I. Rashba. Combined resonance in semiconductors. *Soviet Physics Uspekhi*, 7(6):823, 1965. ISSN 0038-5670. doi: 10.1070/PU1965v007n06ABEH003687. URL `http://iopscience.iop.org/article/10.1070/PU1965v007n06ABEH003687/meta`. Publisher: IOP Publishing.

[37] Peng Li, James Kally, Steven S.-L. Zhang, Timothy Pillsbury, Jinjun Ding, Gyorgy Csaba, Junjia Ding, J. S. Jiang, Yunzhi Liu, Robert Sinclair, Chong Bi, August DeMann, Gaurab Rimal, Wei Zhang, Stuart B. Field, Jinke Tang, Weigang Wang, Olle G. Heinonen, Valentine Novosad, Axel Hoffmann, Nitin Samarth, and Mingzhong Wu. Magnetization switching using topological surface states. *Science Advances*, 5(8):eaaw3415, August 2019. ISSN 2375-2548. doi: 10.1126/sciadv.aaw3415. URL `http://advances.sciencemag.org/content/5/8/eaaw3415`. Publisher: American Association for the Advancement of Science Section: Research Article.

[38] Hailong Wang, James Kally, Joon Sue Lee, Tao Liu, Houchen Chang, Danielle Reifsnyder Hickey, K. Andre Mkhoyan, Mingzhong Wu, Anthony Richardella, and Nitin Samarth. Surface-State-Dominated Spin-Charge Current Conversion in Topological-Insulator–Ferromagnetic-Insulator Heterostructures. *Physical Review Letters*, 117(7):076601, August 2016. doi: 10.1103/PhysRevLett.117.076601. URL `https://link.aps.org/doi/10.1103/PhysRevLett.117.076601`.

[39] Michael A. McGuire, Hemant Dixit, Valentino R. Cooper, and Brian C. Sales. Coupling of Crystal Structure and Magnetism in the Layered, Ferromagnetic Insulator CrI $_3$. *Chemistry of Materials*, 27(2):612–620, January 2015. ISSN 0897-4756, 1520-5002. doi: 10.1021/cm504242t. URL `http://pubs.acs.org/doi/10.1021/cm504242t`.

[40] Bevin Huang, Genevieve Clark, Efrén Navarro-Moratalla, Dahlia R. Klein, Ran Cheng, Kyle L. Seyler, Ding Zhong, Emma Schmidgall, Michael A. McGuire, David H. Cobden, Wang Yao, Di Xiao, Pablo Jarillo-Herrero, and Xiaodong Xu. Layer-dependent ferromagnetism in a van der Waals crystal down to the monolayer limit. *Nature*, 546(7657):270–273, June 2017. ISSN 1476-4687. doi: 10.1038/nature22391. URL `http://www.nature.com/articles/nature22391`.

[41] Bevin Huang, Genevieve Clark, Dahlia R. Klein, David MacNeill, Efrén Navarro-Moratalla, Kyle L. Seyler, Nathan Wilson, Michael A. McGuire, David H. Cobden, Di Xiao, Wang Yao, Pablo Jarillo-Herrero, and Xiaodong Xu. Electrical control of 2D magnetism in bilayer CrI 3. *Nature Nanotechnology*, 13(7):544–548, July 2018. ISSN 1748-3395. doi: 10.1038/s41565-018-0121-3. URL `http://www.nature.com/articles/s41565-018-0121-3`. Number: 7 Publisher: Nature Publishing Group.

[42] Cheng Gong, Lin Li, Zhenglu Li, Huiwen Ji, Alex Stern, Yang Xia, Ting Cao, Wei Bao, Chenzhe Wang, Yuan Wang, Z. Q. Qiu, R. J. Cava, Steven G. Louie, Jing Xia, and Xiang Zhang. Discovery of intrinsic ferromagnetism in two-dimensional van der Waals crystals. *Nature*, 546 (7657):265–269, June 2017. ISSN 0028-0836, 1476-4687. doi: 10.1038/nature22060. URL `http://www.nature.com/articles/nature22060`.

[43] Johannes Frantti, Yukari Fujioka, Christopher Rouleau, Alexandra Steffen, Alexander Puretzky, Nickolay Lavrik, Ilia N. Ivanov, and Harry M. Meyer. In Quest of a Ferromagnetic Insulator: Structure-Controlled Magnetism in Mg–Ti–O Thin Films. *The Journal of Physical Chemistry C*, 123(32):19970–19978, August 2019. ISSN 1932-7447. doi: 10.1021/acs.jpcc.9b05189. URL `https://doi.org/10.1021/acs.jpcc.9b05189`. Publisher: American Chemical Society.

[44] Baiqing Lv, Tian Qian, and Hong Ding. Angle-resolved photoemission spectroscopy and its application to topological materials. *Nature Reviews Physics*, 1(10):609–626, October 2019. ISSN 2522-5820. doi: 10.1038/s42254-019-0088-5. URL `http://www.nature.com/articles/s42254-019-0088-5`. Number: 10 Publisher: Nature Publishing Group.

[45] Akinori Nishide, Alexey A. Taskin, Yasuo Takeichi, Taichi Okuda, Akito Kakizaki, Toru Hirahara, Kan Nakatsuji, Fumio Komori, Yoichi Ando, and Iwao Matsuda. Direct mapping of the spin-filtered surface bands of a three-dimensional quantum spin Hall insulator. *Physical Review B*, 81(4):041309, January 2010. ISSN 1098-0121, 1550-235X. doi: 10.1103/PhysRevB.81.041309. URL `https://link.aps.org/doi/10.1103/PhysRevB.81.041309`.

[46] Pedram Roushan, Jungpil Seo, Colin V. Parker, Y. S. Hor, D. Hsieh, Dong Qian, Anthony Richardella, M. Z. Hasan, R. J. Cava, and Ali Yazdani. Topological surface states protected from backscattering by chiral spin texture. *Nature*, 460(7259):1106–1109, August 2009. ISSN 1476-4687. doi: 10.1038/nature08308. URL `http://www.nature.com/articles/nature08308`.

[47] A. A. Taskin and Yoichi Ando. Quantum oscillations in a topological insulator $Bi_{1-x}Sb_x$. *Physical Review B*, 80(8):085303, August 2009. ISSN 1098-0121, 1550-235X. doi: 10.1103/PhysRevB.80.085303. URL `https://link.aps.org/doi/10.1103/PhysRevB.80.085303`.